5f resonant emission, as the separation of the two peaks (11 ± 2 eV) is comparable to the value of the spin–orbit coupling (9 eV) of the $5d^9$ configuration in the uranium atom.

The resonance profile is similar to the experimental results for the cross sections of uranium metal.[30] We note that the two spin–orbit components of the uranocene d → f resonance do not have an intensity ratio of 3:2, as might be expected for the $D_{5/2}$:$D_{3/2}$ hole states. The $D_{5/2}$ state has the lower excitation energy as the d orbitals are more than half-filled; however, it gives rise to the weaker of the two resonance peaks. This has been discussed by Wendin[31] for the 5d → 5f resonances of thorium and uranium metal. The experimental profiles have been successfully compared with those predicted by a local-density-based random-phase approximation. The spin–orbit splitting of the occupied levels needed to be included from the beginning. It was found that the coupling transfers oscillator strength and hence intensity from the $D_{5/2}$ level, which has a lower binding energy to the higher energy $D_{3/2}$ level as is also seen in our results.

e_{2u} Band. The behavior of the first ligand band RPPICS has features corresponding to those found in the f band RPPICS, confirming the assignment to the e_{2u} orbital, as, by symmetry, only the ligand-based e_{2u} orbitals can interact with the 5f orbitals of uranium (see Figure 1). The RPPICS plots of this band are shown in Figure 7 and the BRs of the e_{2u} band relative to the e_{2g} band in Figure 8; cross-section behavior of this orbital has clearly been influenced by its substantial metal character. As noted in the discussion of the ligand-based RPPICS, most carbon 2p based orbitals show a rapid falloff in cross section as photon energy is increased (Figure 3). The e_{2u} band in uranocene shows a much slower initial falloff than the e_{2g} band and responds to the delayed maximum in the metal f band cross section in that it also shows a small maximum at 39 eV. The e_{2u} band also shows a striking resonance in the 90–125-eV region. The resonance in the e_{2u} band is almost as strong as that in the metal band, indicating a large covalent contribution of the f orbitals to these ligand orbitals. Recent calculations[18,19] have put the metal contribution to these orbitals at 25–33%, and the magnitudes of the relative intensity changes shown here are in full accord with this substantial metal contribution.

e_{2g} Band. The e_{2g} orbitals cannot interact with the uranium f orbitals, and their RPPICS behavior is essentially that of ligand-based orbitals. By symmetry the e_{2g} orbitals can overlap with vacant metal 6d orbitals, and thus to interpret properly the RPPICS behavior of this band, we would need to establish the cross-section behavior of 6d electrons. Theoretical studies suggest cross-section changes between He I and He II photon energies somewhat similar to those found for H 1s orbitals,[27] though p–d resonance phenomena might be expected around 24- and 34-eV photon energy at which energies the U 6p shell ionizes.

As noted before[8] and confirmed by calculations,[18] the significantly higher IE of the e_{2g} electrons compared with the e_{2u} electrons suggests a substantial covalent interaction between the ring π orbitals and the U 6d orbitals, such that the e_{2g} orbitals lie lower in energy than the e_{2u} orbitals and are a larger source of bonding in uranocene.

Conclusions

Unequivocal assignment of the uranocene photoelectron spectrum has been obtained using synchrotron radiation. Cross-section behavior of the metal f band can be explained in atomic terms, and the intensity changes are mimicked in the first ligand (e_{2u}) band. The correspondence of identifiable features in the metal and e_{2u} band RPPICS provides conclusive spectroscopic evidence for substantial f orbital–e_{2u} covalent stabilization in the complex. The crucial role of 6d orbitals in complex stabilization is also implicit in the assignment.

Acknowledgment. We thank the staff at Daresbury Laboratory for experimental assistance, the SERC for financial support, Lady Margaret Hall, Oxford, for an EPA Cephalosporin Research Fellowship (J.G.B.) and the Dee Corp. for a Scholarship (C.M.R.).

Registry No. Bis([8]annulene)uranium, 1076-26-8.

(30) Cukier, M.; Dhez, P.; Gauthe, B.; Jaegle, P.; Wehenkeland, C.; Combet-Farnoux, F. *J. Phys. (Les Ulis, Fr.)* **1978**, *39*, 2315.
(31) Wendin, G. *Phys. Rev. Lett.* **1984**, *53*, 724.

An Investigation of the Decomposition of Osmium Carbonyl Clusters on Carbon Using Diffuse Reflectance Fourier Transform IR Spectroscopy

Jeremy J. Venter and M. Albert Vannice*

Contribution from the Department of Chemical Engineering, The Pennsylvania State University, University Park, Pennsylvania 16802. *Received July 25, 1988*

Abstract: The thermal decomposition of $Os_3(CO)_{12}$ has been studied for the first time by dispersing this cluster on an oxygen-free carbon support and using diffuse reflectance Fourier transform infrared spectroscopy (DRIFTS). The $Os_3(CO)_{12}$/C clusters decomposed straightforwardly in He, but transformed to $H_4Os_4(CO)_{12}$ during decarbonylation in H_2. First-order rate constants of decomposition in He or H_2 were determined for each cluster and compared to literature values for nucleophilic substitution in solution; they were found to be very similar. The activation energy of decarbonylation of $Os_3(CO)_{12}$ was near 28 kcal/mol in He, while $Os_3(CO)_{12}$ and $H_4Os_4(CO)_{12}$ had values of 30–33 kcal/mol in H_2. Chemisorption and DRIFTS measurements indicated the formation of highly dispersed metallic Os particles on carbon following decomposition at 673 K under either He or H_2. The DRIFTS spectra of CO chemisorbed on the surface of these Os crystallites showed no evidence of positive-valent Os. The turnover frequency (CO molecule/s/site) for CO hydrogenation compared favorably with that reported for reduced Os particles on oxide surfaces, and it was about 100-fold higher than the turnover frequencies associated with stabilized positive-valent Os clusters on oxide suports. The isothermal, integral heat of adsorption of CO was measured calorimetrically at 300 K and found to be 31.3 ± 1.1 kcal/mol. This study also represents part of the first successful application of an IR spectroscopic technique to characterize carbon-supported metal clusters.

Many studies on metal carbonyl clusters (MCC's) in solution and on oxide surfaces have appeared in the literature; however, we have found no investigation of the kinetics associated with the thermal decomposition of any such cluster. These clusters have been placed on a variety of support materials to prepare heterogeneous catalysts, and a number of techniques have been used

0002-7863/89/1511-2377$01.50/0

to characterize the original impregnated clusters[1,2] and the final catalysts obtained after decomposition.[3,4] Infrared (IR) spectroscopy has played a major role in providing information about the interaction between the MCC's and functionalized polymers,[5,6] functionalized oxide surfaces,[7-10] and oxide supports.[11-13] These studies have shown the dependence of the reactions on the nature of the initial cluster and the pretreatment of the support material;[11-13] consequently, these interactions can be used to probe the chemical nature of the solid surface. The studies involving Os clusters have been particularly important because the interacting species have been well-characterized by various authors,[11,14,15] and these Os clusters have exceptionally strong metal–metal and metal–CO bonds.

These MCC's routinely interact with oxygen-containing groups that exist on these oxide surfaces; therefore, reaction pathways occur that do not exist in solution. High surface area carbon supports, however, can not only give stable, highly dispersed metal clusters but also can be heat treated to remove all oxygen-containing functional groups, thereby providing a surface free from these interactions. Unfortunately, the highly opaque nature of carbon has precluded the use of IR spectroscopy to characterize these carbon-supported clusters as is routinely done with oxide-supported carbonyl clusters. However, the development of diffuse reflectance Fourier transform infrared spectroscopy (DRIFTS), together with improved cells to enhance sensitivity and in situ pretreatment capabilities,[16-18] now allows examination of carbon-supported MCC's by an IR technique. This paper describes the application of DRIFTS to quantitatively monitor the kinetics of decomposition of $Os_3(CO)_{12}$ in He or H_2 and obtain rate constants and activation energies. In addition, the state of the small metal crystallites produced from these decomposed clusters was characterized by H_2 and CO chemisorption, DRIFTS spectra of this chemisorbed CO, calorimetric measurements of the CO heat of adsorption, and the determination of their catalytic behavior in the CO hydrogenation reaction.

Experimental Section

Catalyst Preparation. The amorphous carbon black used as a support in this study was CSX-203 from Cabot Corp. (now available as Black Pearls 2000). Sulfur and oxygen were removed from the surface by treatment in H_2 at 1223 K for 12 h,[19] and this high-temperature-treated carbon was then stored in a glovebox to avoid air exposure. Before impregnating the support with the carbonyl cluster, the carbon was heated at 673 K under dynamic vacuum (10^{-4} kPa) for 8 h.

The $Os_3(CO)_{12}$ was prepared from OsO_4 using standard procedures[20] and was dispersed on the carbon by an incipient wetness impregnation technique using dry, degassed CH_2Cl_2 as solvent (20 cm^3/g C). The impregnation was done under nitrogen using standard Schlenk techniques,[21] and the solvent was then removed by evacuating to 10^{-4} kPa for 8 h at 300 K, whereafter the catalyst was transferred and stored in the glovebox. The estimated metal Os loading was 9.1 wt %.

DRIFTS Investigation. The infrared spectra were collected on a N_2-purged Mattson Instruments Sirius 100 FTIR, utilizing an extensively modified version of a Harrick Scientific HVC-DRP diffuse reflectance cell which was coupled to a praying mantis mirror assembly (DRA-2CS, Harrick Scientific). The modifications made to this cell have been discussed in detail.[17] The gas-handling system allowed ultra-high-purity H_2, He, N_2, and CO to be flowed through the DRIFTS samples.[17]

The DRIFTS samples were obtained by mixing the supported catalyst with CaF_2. The ultrapure CaF_2 (Alfa Products, Lot 100185) was calcined in 20 cm^3/min O_2 at 823 K for 24 h, treated in 100 cm^3/min H_2 at 823 K for 24 h, cooled to 300 K, evacuated at 300 K for 10 min, and transferred into the glovebox without air exposure. The Os/C catalyst and CaF_2 were then mixed inside the glovebox using a CaF_2:C dilution ratio of 200:1 and ground with a mortar and pestle until the mixture had a uniform gray color. This diluted Os catalyst was stored in the glovebox, and all samples used for the decarbonylation experiments were obtained from this batch.

The loading of the DRIFTS cell was done inside the glovebox by filling the sample cup with diluted catalyst and smoothing the surface with a spatula. The DRIFTS cell was connected to the FTIR, and the lines were thoroughly evacuated and purged prior to flowing 20 cm^3/min He through the catalyst sample. Initial spectra of the cluster were collected in flowing He at 300 K in order to ensure the presence of the intact cluster.

The rates of decarbonylation were measured in H_2 and also in He flowing at 20 cm^3/min unless otherwise noted. For the case of flowing H_2, the catalyst was purged in 20 cm^3/min H_2 at 300 K for 30 min prior to heating the sample to the desired temperature, which required 2–4 min, at which it was kept for the duration of the decarbonylation experiment (2–24 h). Spectra were collected by averaging 1000 scans with the spectrometer parameters set for a resolution of 4 cm^{-1}.

Following the decarbonylation runs, the catalyst was heated to 673 K in the same gas for 4–10 h, purged at 673 K for 30 min in He, and cooled to 300 K. A background spectrum was then collected in He by averaging 10000 scans. A mixture of CO and He at 0.1 MPa (11 Torr CO) was then admitted into the cell and a sample spectrum was collected, after which the cell was purged for 30 min in He to allow the collection of yet another spectrum, again by averaging 10000 scans.

The Os/C catalyst was also investigated under reaction conditions. The diluted sample was first reduced for 16 h in flowing H_2 at 673 K. Background spectra were then collected at 573, 523, and 473 K. A mixture of H_2 and CO (11 Torr CO) was admitted into the cell at 473 K and flowed at 0.1 MPa for 30 min; then spectra were collected at 473, 523, and 573 K. A second spectrum was collected at 573 K after the catalyst had been exposed to the reactant gases for an additional 11 h. All these spectra were collected by signal-averaging 10000 scans.

The data manipulation consisted of ratioing the sample and background spectra to obtain the transmittance spectra, calculating the absorbance spectra from these data, base-line-correcting the absorbance files, obtaining base-line-corrected transmittance files from these, and finally calculating the diffuse reflectance files (in Kubelka–Munk units) from these base-line-corrected transmittance files. The spectra presented in this paper will all be in Kubelka–Munk (K-M) units, where $KM = (1 - R_0)^2/(2R_0)$ and $R_0 = R(\text{sample})/R(\text{background})$, i.e., the base-line-corrected transmittance function; however, each K-M spectrum was compared to the comparable absorbance spectrum to guarantee that no peaks occurred because of improper base-line correction. The fully decarbonylated sample was used as a background for the decarbonylation spectra, as well as for the spectra of CO chemisorbed on reduced Os particles. The validity of this method of data manipulation is described elsewhere.[18,22]

Chemisorption Measurements. The uptake measurements were made using a stainless steel chemisorption system equipped with a Balzers TSU-171 turbomolecular pump and UHV stainless steel bellows valves (MDC Mfg.). Vacuum was measured by a Granville-Phillips Model 260 Bayard–Alpert ionization gauge. Pressures below 10^{-8} Torr in the manifold and down to 10^{-7} Torr in the adsorption cell were routinely obtained. An MKS Baratron Model 310 high-precision capacitance manometer was used to monitor gas pressures during chemisorption measurements. A more detailed description of the gases and their purification is given elsewhere.[19,23]

(1) Zwart, J.; Snel, R. *J. Mol. Catal.* **1985**, *30*, 305.
(2) Moskovits, M. *Metal Clusters*; Wiley: New York, 1986.
(3) Guczi, L. *Catal. Rev. Sci. Eng.* **1981**, *23*, 329.
(4) Foger, K. *Catal. Sci. Technol.* **1984**, *6*, 228.
(5) Pierantozzi, R.; McQuade, K. J.; Gates, B. C.; Wolf, M.; Knozinger, H.; Ruhmann, W. *J. Am. Chem. Soc.* **1979**, *101*, 5436.
(6) Lieto, J.; Wolf, M.; Matrana, B. A.; Prochazka, M.; Tesche, B.; Knozinger, H.; Gates, B. C. *J. Phys. Chem.* **1985**, *89*, 991.
(7) Castrillo, T.; Knozinger, H.; Wolf, M. *Inorg. Chim. Acta* **1980**, *44*, L235.
(8) Castillo, T.; Knozinger, H.; Wolf, M.; Tesche, B. *J. Mol. Catal.* **1981**, *11*, 151.
(9) Wolf, M.; Knozinger, H.; Tesche, B. *J. Mol. Catal.* **1984**, *25*, 273.
(10) Hemmerick, R.; Kelm, W.; Roper, M. *J. Chem. Soc., Chem. Commun.* **1983**, 428.
(11) Psaro, R.; Dossi, C.; Ugo, R. *J. Mol. Catal.* **1983**, *21*, 331.
(12) Psaro, R.; Ugo, R.; Zanderighi, G. M.; Besson, B.; Smith, A. K.; Basset, J. M. *J. Organomet. Chem.* **1981**, *213*, 215.
(13) Smith, A. K.; Besson, B.; Basset, J. M.; Psaro, R.; Fusi, A.; Ugo, R. *J. Organomet. Chem.* **1980**, *192*, C31.
(14) Basset, J. M.; Choplin, A. *J. Mol. Catal.* **1983**, *21*, 95.
(15) Deeba, M.; Gates, B. C. *J. Catal.* **1981**, *67*, 303.
(16) Venter, J. J.; Vannice, M. A. *J. Am. Chem. Soc.* **1987**, *109*, 6204.
(17) Venter, J. J.; Vannice, M. A. *Appl. Spectrosc.* **1988**, *42*, 1096.
(18) Venter, J. J.; Vannice, M. A. *Carbon* **1988**, *26*, 889.
(19) Kaminsky, M.; Yoon, K. J.; Geoffroy, G. L.; Vannice, M. A. *J. Catal.* **1985**, *91*, 338.
(20) Johnson, B. F. G.; Lewis, J. *Inorg. Synth.* **1976**, *13*, 92.
(21) Schriver, D. F. *The Manipulation of Air Sensitive Compounds*; McGraw-Hill: New York, 1969.
(22) Venter, J. J. Ph.D. Thesis, The Pennsylvania State University, 1988.
(23) Jung, H. J.; Vannice, M. A.; Mulay, L. N.; Stanfield, R. M.; Delgass, W. N. *J. Catal.* **1982**, *76*, 208.

Table I. Chemisorption Measurements on 9.1 wt % Os/C Catalysts Derived from $Os_3(CO)_{12}$

	fresh catalyst		used catalyst	
gas (temp)	uptake (μmol/g cat.)	Co/Os or H/Os	uptake (μmol/g cat.)	CO/Os or H/Os
	LTR			
H_2 (0–200 °C)	45	0.19		
CO (195 K)	16	0.03		
CO (300 K)	211	0.44		
CO (300 K)/CO (195 K)	13.4			
	HTR			
H_2 (0–400 °C)	90	0.38	94	0.39
CO (195 K)	256	0.53	277	0.47
CO (300 K)	330	0.69	287	0.60
CO (300 K)/CO(195 K)	1.3		1.3	

Table II. Kinetic Behavior of Os/C Catalysts Derived from $Os_3(CO)_{12}$

	activity[a] (μ/mol CO/g cat. s)		turnover frequency ($s^{-1} \times 10^3$)		activation energy (kcal/mol)		partial pressure dependency[d]	
	LTR	HTR	LTR[b]	HTR[c]	LTR	HTR	x	y
CO (tot)	0.482	0.395	2.3	1.4	29.7	28.0		
$CO-CO_2$	0.005	0.005	0.02	0.02	25.8	15.8		
CO–HC	0.478	0.390	2.3	1.4	29.7	28.0	1.1	0.0
$CO-CH_4$	0.478	0.390	2.3	1.4	29.7	28.0	1.1	0.0

[a] P = 0.1 MPa, H_2/CO = 3.1, T = 548 K; LTR (low-temperature reduction at 473 K), HTR (high-temperature reduction at 673 K). [b] Based on CO (300 K) assuming $CO/Os_s = 1$. [c] Based on CO (300 K) on used catalyst, $CO/Os_s = 1$. [d] $r = kP_{H_2}{}^x P_{CO}{}^y$, T = 537 K, after HTR.

For chemisorption measurements on the fresh catalyst, 0.4–0.6 g of catalyst was loaded into a Pyrex cell equipped with greaseless, high-vacuum stopcocks and attached to the adsorption apparatus via a high-vacuum, O-ring joint. The fresh catalyst was then subjected to a low-temperature reduction (LTR) by heating the sample in H_2 (40 cm^3/min) to 473 K and reducing at that temperature for 2 h. Chemisorbed CO at both 195 and 300 K was determined using a dual isotherm method,[24] and hydrogen adsorbed during cooling in H_2 to 300 K was measured as described elsewhere.[25,26] Following these measurements, the catalyst was subjected to a high-temperature reduction (HTR) by heating the catalyst in flowing H_2 to 673 K and reducing at this temperature for 16 h. The exact sequence of steps was then followed as for the LTR, but with the sample being reduced at 673 K for 16 h, rather than 473 K for 2 h. Hence, the hydrogen adsorbed was determined after cooling in H_2 to 300 K. Chemisorption measurements were also done on the used samples after the kinetic studies using only the HTR pretreatment as discussed above. In all cases, the catalyst was transferred and stored in the glovebox following adsorption measurements.

Kinetic Measurements. The kinetic data were obtained at 1 atm under differential conditions using a glass, plug-flow microreactor.[23] Catalyst samples were approximately 0.5–0.8 g, and CO conversions were kept below 10% in order to avoid heat and mass transfer limitations.

Catalyst samples were loaded into a Pyrex reactor cell in a glovebox, transferred to the reactor system, and purged in He with no air exposure. The catalyst was then purged in H_2 at 300 K prior to subjecting it to a LTR treatment. Activity measurements were made between 473 and 573 K using a bracketing technique involving a 20-min exposure to pure H_2 between each set of data points to avoid deactivation.[27,28] Following HTR, additional activity measurements were made using the same procedure as above, and partial pressure analyses were performed using He as a diluent in the feed stream. Following the kinetic measurements, the catalytic reactor was sealed and transferred into the glovebox where the catalyst was stored.

Calorimetric Measurements. The isothermal energy changes during adsorption of CO were measured using a modified Perkin-Elmer DSC-2C differential scanning calorimeter with a water-cooled thermal block and a gas-handling system to control the flows of H_2, He, CO, and Ar and provide a switching capability between two streams.[29,30] The only additional modification that was made was the installation of a small N_2-purged glovebox onto the DSC which allowed the transfer of samples from the glovebox into the DSC with no air exposure.

In order to avoid the possible volatilization of carbonyl clusters during their initial decomposition in the DSC, special procedures were developed not only to circumvent this problem, but also to ensure the determination of reproducible heats of adsorption (Q_{ad}). A rather large amount of carbon-supported catalyst (1–2 g) was loaded into a Pyrex cell, connected to the chemisorption apparatus, subjected to HTR, cooled to 300 K, evacuated for 10 min, and transferred into the glovebox. This single, reduced sample was then used as the source of all the DSC samples.

The DSC sample pans were washed and handled as described elsewhere[31] and transferred into the glovebox where both the chemisorption cell (0.2–0.5 g) and the DSC sampling pan (0.10–0.15 g) were loaded at the same time from the same batch of reduced catalyst. The DSC sample was then transferred without air exposure to the DSC and purged in 40 cm^3/min Ar for 30 min prior to switching to a flow of 40 cm^3/min H_2 and 0.7 cm^3/min He. The cell was purged for 10 min, heated to 673 K at a rate of 10 K/min, and reduced at 673 K for 16 h. The catalyst was then purged in a stream of 40 cm^3/min Ar and 0.7 cm^3/min He for 3 h and cooled to 300 K at 40 K/min. After purging at 300 K for 10 min following thermal equilibration, the gas was switched to a stream consisting of 36 cm^3/min Ar, 4 cm^3/min CO, and 0.7 cm^3/min He, and the heat evolution was monitored on the recorder until the base line was restored (5–10 min). The sample was then purged in the Ar/He stream for 5 min after which an initial reversible adsorption peak was measured by reintroducing CO. The sample was then flushed for 3 h in the Ar/He stream after which a second exotherm, associated with reversible CO adsorption, was measured. Following these measurements, the sample was purged in the Ar/He stream for 30 min after which the entire procedure was repeated. This cycle was typically repeated two or three times for two different samples in order to determine the reproducibility of measured heats.

Results

Chemisorption. The metal weight loading was estimated to be 9.1 wt % Os from the impregnation. The weight loading determined by slow ashing of the catalyst was only 2.6 wt % due to volatilization of OsO_4 leading to impossibly high apparent dispersions of well above unity.

The chemisorption results are listed in Table I. The CO chemisorption value at 195 K after an initial LTR seems unusually low, as though the $Os_3(CO)_{12}$ clusters, or carbonyl derivatives thereof, were incompletely decomposed.[11,12] The low hydrogen uptake is consistent with this conclusion. The CO chemisorption at 300 K increased markedly after the second LTR, indicating that a larger fraction of the cluster had decomposed. All chemisorption values after HTR were significantly higher, although

(24) Emmett, P. H.; Brunauer, S. *J. Am. Chem. Soc.* **1937**, *59*, 310.
(25) Chen, A.; Kaminsky, M.; Geoffroy, G. L.; Vannice, M. A. *J. Phys. Chem.* **1986**, *90*, 4810.
(26) Venter, J. J.; Kaminsky, M.; Geoffroy, G. L.; Vannice, M. A. *J. Catal.* **1987**, *103*, 450.
(27) Vannice, M. A. *J. Catal.* **1975**, *37*, 449.
(28) Vannice, M. A. *J. Catal.* **1977**, *50*, 228.
(29) Sen, B.; Chou, P.; Vannice, M. A. *J. Catal.* **1986**, *101*, 517.
(30) Chou, P.; Vannice, M. A. *J. Catal.* **1987**, *104*, 1.
(31) Chou, P.; Vannice, M. A. *J. Catal.* **1987**, *104*, 17.

Table III. Heats of Adsorption of CO on Reduced Carbon-Supported Os Derived from $Os_3(CO)_{12}$

run no.	heat released (mcal/g cat.)	irreversible chemisorption (μmol/g cat.)	heat of adsorption (kcal/mol)	dispersion (CO/Os)
		Sample 1		
1		265		0.55
2	7966	271	29.4	0.56
3	8636	244	32.2	0.51
		Sample 2		
1	8815	276	31.9	0.58
2	8503	267	31.8	0.56
			31.3 ± 1.1[a]	0.55

[a] Average ± standard deviation.

the hydrogen uptake was lower than either CO uptake. The CO chemisorptions at 195 and 300 K were very similar, as expected for nondissociative adsorption of CO with limited subcarbonyl formation, if any, at 300 K.[32-36]

Chemisorption on the used catalysts gave closer agreement between the H_2 and CO uptakes, and the room-temperature CO uptake was again somewhat higher than that at 195 K. These chemisorption values were, on the average, only 10% less than those for the fresh sample, indicating that minimal sintering occurred during the CO hydrogenation reaction and that the reduced Os clusters were quite stable. The dispersions were near 50% or higher based on CO chemisorption.

Kinetic Measurements. The kinetic data are summarized in Table II. An active catalyst was obtained after only a LTR, and the activity decreased slightly following a HTR indicative of the decrease in surface area. The catalyst produced only CH_4 and CO_2 in measurable quantities; hence rates of CO conversion to hydrocarbons (HC) were equal to those for methanation. The activation energies for the formation of CH_4 after either LTR or HTR were essentially the same, but the values for CO_2 formation changed markedly. The partial pressure analysis showed a first-order dependence on H_2 and a zero-order dependence on CO.

Calorimetric Measurements. The integral, isothermal heats of adsorption of CO are shown in Table III together with the CO chemisorption values. The chemisorption uptakes were in excellent agreement, indicating once again the resistance to sintering of the Os particles, and they were very reproducible from sample to sample. The measured heats of adsorption were also in good agreement, and the average CO heat of adsorption was 31.3 ± 1.1 kcal/g-mol of CO.

DRIFTS Measurements. Prior to the decarbonylation experiments, the spectrum of $Os_3(CO)_{12}$ dispersed on this carbon was recorded in flowing He. The initial peak positions remained unaltered throughout the study and had frequencies at 2068, 2031, 2015, and 2002 cm^{-1}, in excellent agreement with reported values in Table IV for the cluster in solution.[37-57] The catalyst was then heated in either He or H_2 to a constant temperature and decarbonylated, with a typical example shown in Figure 1 for $Os_3(CO)_{12}$ in He at 363 K. Note that the initial spectrum at 363 K exhibited the same frequencies as reported for the cluster in solution, and that these frequencies were the only ones observed for the duration of the decarbonylation experiment, which was 1270 min in this

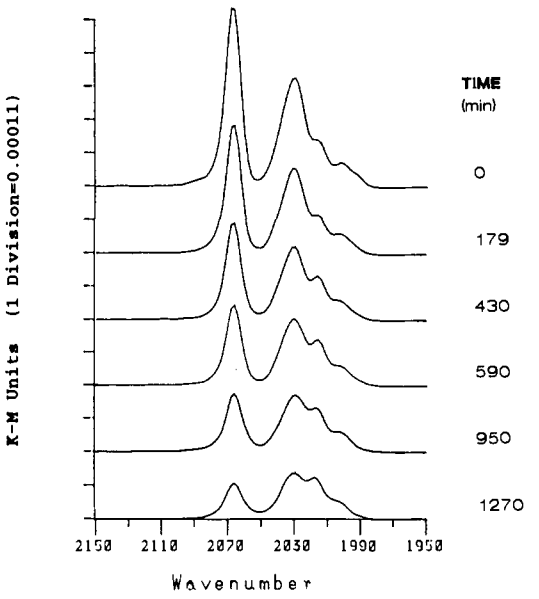

Figure 1. Spectra of carbon-supported $Os_3(CO)_{12}$ after various times in He at 363 K. The principal IR bands are at 2066, 2031, 2016, and 2002 cm^{-1}.

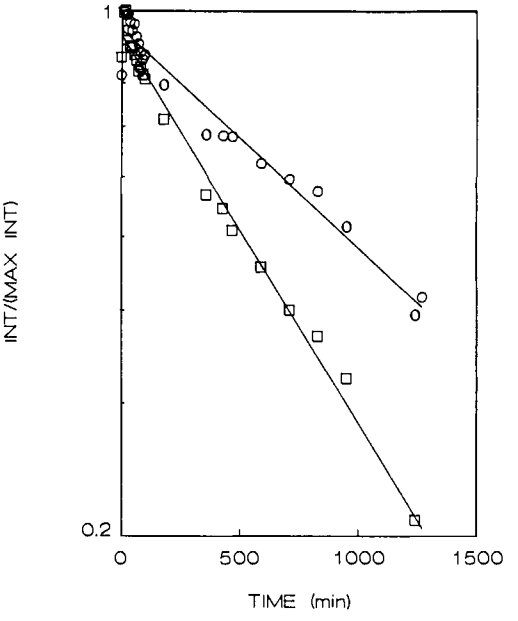

Figure 2. Rates of decarbonylation of carbon-supported $Os_3(CO)_{12}$ in He at 363 K: ○, band at 2066 cm^{-1}; □, band at 2031 cm^{-1}.

(32) Prestridge, E. B.; Via, G. H.; Sinfelt, J. H. *J. Catal.* **1977**, *50*, 115.
(33) Sinfelt, J. H. *J. Catal.* **1973**, *29*, 308.
(34) Via, G. H.; Sinfelt, J. H.; Lytle, F. W. *J. Chem. Phys.* **1979**, *71*, 690.
(35) Bell, A. T. *Catal. Rev.* **1981**, *23*, 203.
(36) Foger, K. *Catal. Sci. Technol.* **1984**, *6*, 228.
(37) Calderazzo, F.; L'Eplattenier, F. *Inorg. Chem.* **1967**, *6*, 1220.
(38) Barth, R.; Gates, B. C.; Zhao, Y.; Knozinger, H.; Hulse, J. *J. Catal.* **1983**, *82*, 147.
(39) Crawford, J. E.; Melson, G. A.; Makovsky, L. E.; Brown, F. R. *J. Catal.* **1983**, *83*, 454.
(40) Watson, P. L.; Schrader, G. L. *J. Mol. Catal.* **1980**, *9*, 129.
(41) Poliakoff, M.; Turner, J. J. *J. Chem. Soc. A* **1971**, 654.
(42) Poliakoff, M.; Turner, J. J. *J. Chem. Soc., Chem. Commun.* **1970**, 1008.
(43) Lamb, H. H.; Gates, B. C. *J. Am. Chem. Soc.* **1986**, *108*, 81.
(44) Jordan, R. F.; Norton, J. R. *J. Am. Chem. Soc.* **1982**, *104*, 1255.
(45) Effa, J. B. N.; Lieto, J.; Aune, J. P. *J. Mol. Catal.* **1982**, *15*, 367.
(46) Knox, S. A. R.; Koepke, J. W.; Andrews, M. A.; Kaesz, H. D. *J. Am. Chem. Soc.* **1975**, *97*, 3942.
(47) Brown, S. C.; Evans, J. *J. Chem. Soc., Chem. Commun.* **1978**, 1063.
(48) Eady, C. R.; Johnson, B. F. G.; Lewis, J. J. *J. Organomet. Chem.* **1973**, *57*, C84.
(49) Moss, J. R.; Graham, W. A. G. *J. Organomet. Chem.* **1970**, *23*, C47.
(50) Kaesz, H. D.; Knox, S. A. R.; Koepke, J. W.; Saillant, R. B. *J. Chem. Soc., Chem. Commun.* **1971**, 477.
(51) Johnson, B. F. G.; Lewis, J.; Raithby, P. R.; Sheldrick, G. M.; Wong, K.; McPartlin, M. *J. Chem. Soc., Dalton Trans.* **1978**, 673.
(52) Catrillo, T.; Knozinger, K.; Wolf, M. *Inorg. Chim. Acta* **1980**, *45*, L235.
(53) Deeba, M.; Scott, J. P.; Barth, R.; Gates, B. C. *J. Catal.* **1981**, *71*, 373.
(54) Besson, B.; Moraweck, B.; Smith, A. K.; Basset, J. M. *J. Chem. Soc., Chem. Commun.* **1980**, 569.
(55) Krause, T. R.; Davies, M. E.; Lieto, J.; Gates, B. C. *J. Catal.* **1985**, *94*, 195.
(56) Deeming, A. J.; Johnson, B. F. G.; Lewis, J. *J. Chem. Soc. A* **1970**, 897.
(57) Tripathi, S. C.; Srivastava, S. C.; Mani, R. P.; Shrimal, A. K. *Inorg. Chim. Acta* **1975**, *15*, 249.

Table IV. Summary of Reported IR Bands for Osmium Carbonyls in Solution

cluster	IR bands					ref
$Os(CO)_5$	2034[a]	1991				
$Os_3(CO)_{12}$	2068	2035–2034	2014–2013	2003–1999		37
$Os_6(CO)_8$	2109	2081	2061	2039	2022	38–42
$H_2Os(CO)_4$	2143–2132	2067–2060	2055–2050	2050–2038		43, 44
$H_2Os_2(CO)_8$	2129	2089	2055	2029	2012	44
$H_2Os_3(CO)_{10}$	2079–2076	2066–2063	2026–2020	2011–2002	1989	12, 13, 45, 46
$H_4Os_4(CO)_{12}$	2092–2085	2074–2065	2026–2020	2002–1980		12, 13, 45, 46
$H_2Os_4(CO)_{13}$	2085	2068	2059	2021	2005	46–51
$H_2Os_5(CO)_{16}$	2126	2088	2066	2053	2045–2038	48
$H_2Os_6(CO)_{18}$	2084	2078	2049	2042		48
$HOs(CO)_4^-$	2010–2006	1975	1952	1883–1880		44
$HOs_2(CO)_8^-$	2085	2077	2026	1996	1935	1882	44
$HOs_3(CO)_{10}^-$	2077–2066	2064–2057	2033–2021	2018–2004	1998–1989	12, 13, 48, 52–54
$H_3Os_4(CO)_{12}^-$	2047	2021	1999	1974		51, 55
$Os_3(CO)_{11}^{2-}$	2040	1970	1950	1890		11
$Os_3(CO)_{11}L$	2056–2054	2034–2032	2022–2021	2001–2000	11988–1985	56, 57
$Os_3(CO)_{10}L_2$	2083–2081	2024–2021	2002–2000	1965–1960	1954–1940	56, 57
$Os_3(CO)_9L_3$	1999–1987	1974–1976	1938–1944			57

[a] Underlined numbers represent major bands.

Table V. Activation Energies and Rate Constants for Decarbonylation of Os Clusters in H_2 and He at 350 K

cluster (IR band) (cm^{-1})	rate constant of decarbonylation (350 K, min^{-1})		activation energy of decarbonylation (kcal/mol)	
	He	H_2	He	He_2
$Os_3(CO)_{12}$(2066)	0.00015	0.00026	27.3	32.5
$Os_3(CO)_{12}$(2031)	0.00015	0.00020	28.8	32.5
$H_4Os_4(CO)_{12}$(2017)		0.00018		29.8

particular case, indicating the cluster decomposed without the formation of a more stable carbonyl species. Assuming a first-order rate process, as expected for ligand dissociation or metal–metal bond cleavage reactions,[58] the rate constants for decarbonylation were determined from plots of the decrease of peak intensities at 2066 and 2031 cm^{-1} as a function of time, as shown in Figure 2, and they are given in Table V. The intensity decay for both these frequencies, where I_{max} represents the maximum intensity obtained, is described well by first-order kinetics. The observation that the first-order plots do not always go through the origin is most likely due to initial temperature overshoot and oscillations allowed by the proportional temperature controller during the rapid increase in sample temperature, and is not believed to have any mechanistic significance.

The decarbonylation of $Os_3(CO)_{12}$ on carbon in H_2 at 363 K is shown in Figure 3. Again the initial spectrum was similar to that of the carbonyl in solution, but in H_2 a simple decarbonylation of the starting cluster was not observed. Instead, a simultaneous decomposition of $Os_3(CO)_{12}$, as shown by the diminishing intensities of the 2066- and 2031-cm^{-1} bands, and the formation of a new species (S1), as shown by the growing intensity of the 2017-cm^{-1} band, were observed. This behavior in H_2 was not limited to decarbonylation at 363 K but was observed for all experiments between 363 and 433 K, with both the formation and decomposition of S1 increasing rapidly with temperature. As another example, the decarbonylation at 393 K is shown in Figure 4, where the essential process remained unaltered but proceeded more rapidly.

The determination of representative rate constants becomes complicated when IR-active decomposition products are formed which give overlapping bands in the regions of the precursor bands. Ideally, the two species should be spectrally deconvoluted, which would allow the investigation of both species independently, but the current computer capabilities unfortunately do not allow the deconvolution of peaks. Consequently, this set of consecutive

(58) Geoffroy, G. L.; Wrighton, M. S. *Organometallic Photochemistry*; Academic Press: New York, 1979.

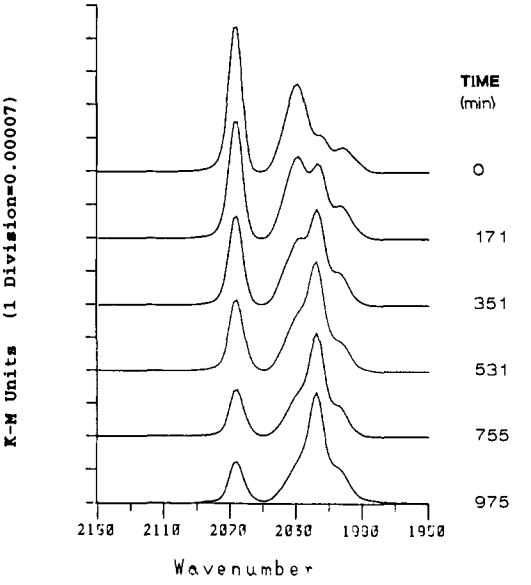

Figure 3. Spectra of carbon-supported $Os_3(CO)_{12}$ after various times in H_2 at 363 K. The principal IR bands are at 2066, 2031, and 2017 cm^{-1}.

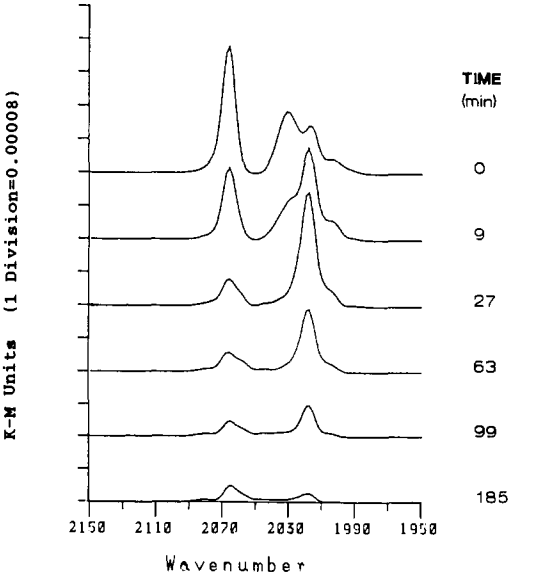

Figure 4. Spectra of carbon-supported $Os_3(CO)_{12}$ after various times in H_2 at 393 K. The principal IR bands are at 2066, 2031, and 2017 cm^{-1}.

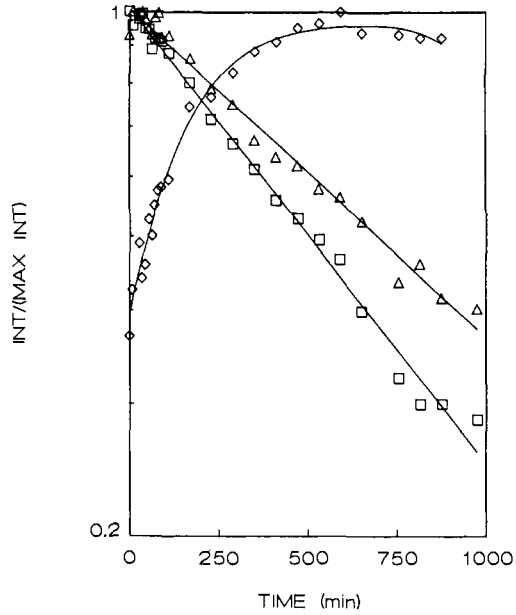

Figure 5. Rates of decarbonylation of carbon-supported $Os_3(CO)_{12}$ in H_2 at 363 K: ○, band at 2066 cm^{-1}; □, band at 2031 cm^{-1}; ◇, band at 2017 cm^{-1}.

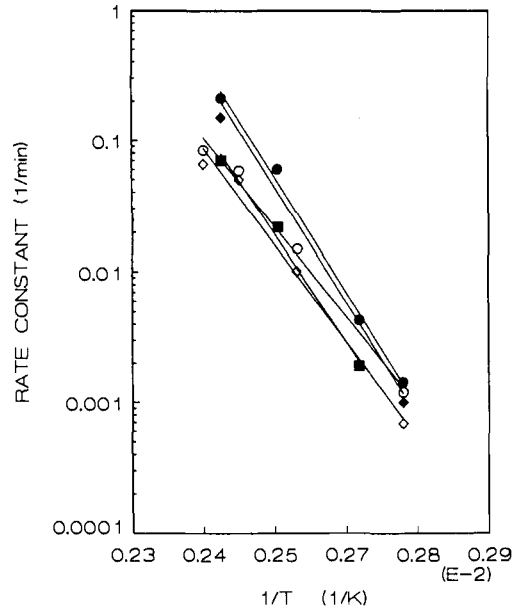

Figure 6. Arrhenius plots for the decarbonylation of carbon-supported $Os_3(CO)_{12}$: ○, 2066-cm^{-1} band in He; ◇, 2031-cm^{-1} band in He; ●, 2061-cm^{-1} band in H_2; ◆, 2031-cm^{-1} band in H_2; ■, 2017-cm^{-1} band in H_2 [$H_4Os_4(CO)_{12}$].

reactions, assumed to be first-order, can be studied by either assuming an irreversible first-order decomposition process and determining the rate constants from initial slopes, or the IR peak intensity variation can be modelled as a reversible first-order process. The latter method allows for the correction of residual background peaks by choosing a residual intensity at the time when the original cluster finally disappears. Both procedures were used to determine rate constants for the worst case (the decarbonylation of $Os_3(CO)_{12}$ in H_2 at 363 K where the formation of S1 was the most noticable) in order to determine the maximum variation that could be observed. These results showed that the rate constants differed by no more than 20–40%, while the calculated activation energies remained the same;[22] consequently, all results were obtained from initial rates assuming irreversible, first-order kinetics.

First-order decarbonylation rates in H_2 at 363 K are shown in Figure 5, which clearly shows that the decomposition of the $Os_3(CO)_{12}$ cluster, as represented by the 2066- and 2031-cm^{-1} bands, was well-described by this rate equation. Although it is not as clearly shown at 363 K as at higher temperatures, the S1 species also decomposed, giving a maximum intensity with time; this process was also described by first-order kinetics.

The rate constants obtained from the slopes of these plots were used to determine the activation energies of decarbonylation from the Arrhenius plots in Figure 6. These activation energies, together with the values of the rate constants at 350 K, are listed in Table V. The activation energies in He associated with the loss of either the 2066- or the 2031-cm^{-1} band were in good agreement, as were the values obtained in H_2; however, the values in H_2 were slightly higher than those obtained in He. The rates of decomposition in H_2 were slightly higher than those obtained in He, but the rates for all bands were near 0.0002 min^{-1} at 350 K.

CO Adsorption. Following the decarbonylation runs, the catalyst was heated to 673 K in either H_2 or He, kept at 673 K in this gas, and purged in He at 673 K for 30 min, after which the CO chemisorption run was conducted at 300 K by exposing the sample 11 Torr CO for 2 h, then flushing for 30 min. The spectrum for adsorbed CO obtained in flowing He after the catalyst was reduced in flowing H_2 at 673 K for 10 h is shown in Figure 7a. The observed frequency at 2037 cm^{-1} is in good agreement with values obtained for CO adsorbed on SiO_2-supported Os,[12] Al_2O_3-supported Os,[12,59] and Os films,[60] and it is associated with linearly

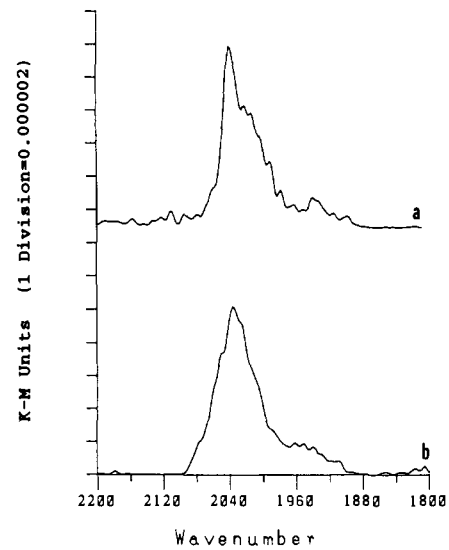

Figure 7. Spectra of CO adsorbed on Os crystallites at 300 K: (a) following a 10-h reduction in H_2 at 673 K; (b) following a 4-h treatment in He at 673 K.

adsorbed CO on metallic Os. The spectrum obtained for CO adsorbed at 300 K on the fully decomposed Os/C catalyst after treatment at 673 K in He for 4 h is shown in Figure 7b. A single absorption band at 2035 cm^{-1} was obtained, again in good agreement with reported values for CO adsorbed on zerovalent Os. Both spectra indicate the presence of metallic Os particles and show that no oxidation of these Os atoms occurs on these cleaned, oxygen-free carbon surfaces.

Reaction Conditions. Spectra obtained under CO hydrogenation reaction conditions (11 Torr CO in 749 Torr H_2) are shown in Figure 8. Several general statements can be made. In all four spectra three sets of bands appeared, namely, those of gas-phase CO_2 (2300–2400 cm^{-1}), adsorbed CO (1950–2030 cm^{-1}), and CH_x species (2800–3000 cm^{-1}). The gas-phase CO bands were subtracted using previously collected gas-phase CO spectra. The gas-phase CO_2 concentration increased as the temperature increased, as expected. The intensity of the adsorbed CO decreased

(59) Knozinger, H.; Zhao, Y.; Tesche, B.; Barth, R.; Epstein, R.; Gates, B. C.; Scott, J. P. *Faraday Discuss. Chem. Soc.* **1982**, *72*, 53.

(60) Collier, G.; Hunt, D. J.; Jackson, S. D.; Moyes, R. B.; Pickering, I. A.; Wells, P. B. *J. Catal.* **1983**, *80*, 154.

Table VI. Comparison of Kinetic Parameters for CO Hydrogenation over Supported Os Catalysts

precursor	support	weight %	reported activity				products	calculated[b] TOF (s^{-1})	E_a (kcal/mol)	ref
			T (K)	P (atm)	H_2/CO	TOF[a] (s^{-1})				
$Os_3(CO)_{12}$	C(LTR)	9.1	548	1	3	2.3×10^{-3}	C_1	2.3×10^{-3}	30	this work
	C(HTR)	9.1	548	1	3	1.5×10^{-3}	C_1	1.5×10^{-3}	28	this work
$Os_3(CO)_{12}$	SiO_2	<1	473	10	1	3×10^{-4}	C_1–C_4	5×10^{-3}		99
$Os_3(CO)_{12}$	MgO	<1	573	31.8	4	8×10^{-4}	C_1–C_3	6×10^{-6}		53
H_2OsCl_6	Al_2O_3	<1	606	1	3	2.5×10^{-4}	C_1	2×10^{-5}		59
$Os_3(CO)_{12}$	Al_2O_3	<1	606	1	3	1.5×10^{-9}	C_1–C_3	1×10^{-5}		59
$H_4Os_4(CO)_{12}$	Al_2O_3	<1	473	32	3	1.3×10^{-4}	C_1–C_3	3×10^{-5}		59
$Os_3(CO)_{12}$	Al_2O_3	<1	523	1	3	6×10^{-5}	C_1	2×10^{-4}		100
$Os_3(CO)_{12}$	Al_2O_3	<1	523	1	3	5×10^{-6}	C_1	2×10^{-5}		100
$H_2Os(CO)_5$	MgO	<1	548	10	1	1.5×10^{-4}	C_1–C_4	2×10^{-5}		43
$Os(CO)_5$	Al_2O_3	<1	548	10	1	2.9×10^{-4}	C_1	4×10^{-4}	16	101
$Os_3(CO)_{12}$	Al_2O_3	2	605	1	3	5.7×10^{-5}	C_1	4×10^{-6}	23	102,103
$Os_3(CO)_{12}$	SiO_2	2	605	1	3	1.2×10^{-2}	C_1	8×10^{-4}	18	102,103
$Os_3(CO)_{12}$	TiO_2	2	605	1	3	1×10^{-2}	C_1	7×10^{-4}	22	102,103
$Os_6(CO)_{18}$	Al_2O_3	2	605	1	3	7.6×10^{-6}	C_1	6×10^{-7}	28	102,103
$Os_6(CO)_{18}$	SiO_2	2	605	1	3	4.3×10^{-2}	C_1	2.9×10^{-3}	18	102,103
$Os_6(CO)_{18}$	TiO_2	2	605	1	3	8.3×10^{-4}	C_1	6×10^{-5}	19	102,103

[a] TOF for the conversion of CO to hydrocarbons (molecule $CO \cdot s^{-1} \cdot Os^{-1}_{surf}$). [b] T = 548 K, P = 101.3 kPa, H_2:CO = 3:1, using $r = A \exp(31\,000/RT)\, R^1_{H_2}\, P^0_{CO}$.

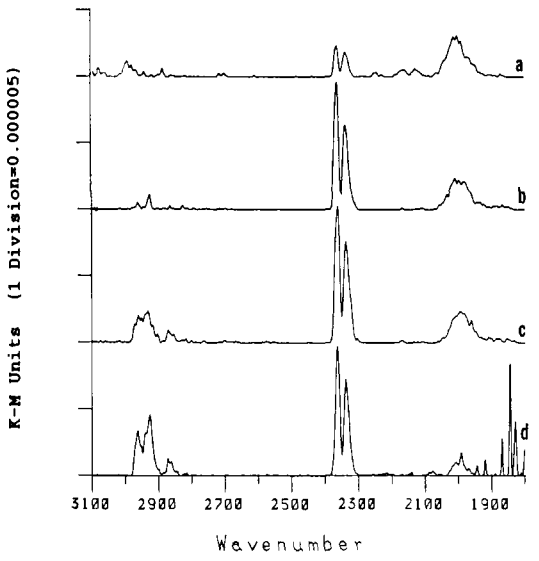

Figure 8. Spectra of carbon-supported $Os_3(CO)_{12}$ under reaction conditions of 11 Torr CO in 749 Torr H_2: (a) At 473 K after 90 min; (b) at 523 K after an additional 90 min; (c) at 573 K after an additional 90 min; (d) at 573 K after an additional 9 h.

with increasing temperature, while the CH_x intensities increased with increasing time on-stream. These intensities were noticeably enhanced after an additional 11 h on-stream at 573 K. The adsorbed CO bands were at lower frequencies than those observed at 300 K, and indicated that strongly adsorbed CO dominated the surface at these elevated temperatures. As seen most clearly in Figure 8d, the bands attributed to various CH_x bonds consisted of two doublets: a set at 2872 and 2962 cm^{-1} in close agreement with reported values for methyl groups at 2875 and 2960 cm^{-1}, and a set at 2862 and 2927 cm^{-1} which is close to reported values of 2850 and 2925 cm^{-1} for methylene groups.[61,62]

Discussion

The use of carbon to prepare supported metal catalysts is increasing;[19,23,25,26,63-73] one reason for this is that amorphous carbons can be prepared with high surface areas of over 1000 m^2/g which can stabilize very small (<2 nm) Ru, Co, Fe, and Mn particles.[19,23,25,26,63] Another is that these carbons can be dehydroxylated to prevent oxidation of supported metals; such carbon-supported metals have resulted in highly dispersed, very active CO hydrogenation catalysts.[19,23,25,26,63] Preparation of these metal systems using metal carbonyl clusters (MCC's) provides metals in a zero-oxidation state, gives stoichiometric metal ratios when mixed-metal clusters are used, and allows easy promotion by group IA metals when anionic clusters are used.[19,25,26,64] These clusters have shown interesting catalytic behavior in the CO hydrogenation reaction when placed on oxide supports[26,74-80] and on carbon.[19,23,25,26,63,64]

The study of the chemistry of these clusters on carbon supports by IR spectroscopy has not been possible because carbon is an excellent black-body absorber of energy. To data, IR studies of these opaque carbonaceous materials have been limited to surface functional groups on carbon blacks,[81,82] activated carbons,[83-85] carbon films,[86,87] coals,[88,89] and carbonaceous electrode materials.[90] No IR investigation of C-supported metals has been reported

(61) King, D. L. *J. Catal.* **1980**, *61*, 77.
(62) Tipson, R. S. *Infrared Spectroscopy of Carbohydrates*, NBS Monograph 110; National Bureau of Standards: Washington, D.C., 1968.
(63) Niemantsverdriet, J. W.; van der Kraan, A. M.; Delgass, W. N.; Vannice, M. A. *J. Phys. Chem.* **1985**, *89*, 67.
(64) Venter, J. J.; Kaminsky, M.; Geoffroy, G. L.; Vannice, M. A. *J. Catal.* **1987**, *105*, 155.
(65) Phillips, J.; Clausen, B.; Dumesic, J. A. *J. Phys. Chem.* **1980**, *84*, 1814.
(66) Phillips, J.; Dumesic, J. A. *Appl. Catal.* **1984**, *9*, 1.
(67) Lin, S. C.; Phillips, J. *J. Appl. Phys.* **1985**, *58*, 1943.
(68) Gatte, R. R.; Phillips, J. P. *J. Catal.* **1987**, *104*, 365.
(69) Bartholomew, C. H.; Boudart, M. *J. Catal.* **1973**, *29*, 278.
(70) Jones, V. K.; Neubauer, L. R.; Bartholomew, C. H. *J. Phys. Chem.* **1986**, *90*, 4832.
(71) Tau, L. M.; Bennett, C. O. *J. Phys. Chem.* **1986**, *90*, 4825.
(72) Reinoso, F. R.; Ramos, I. R.; Castilla, C. M.; Ruiz, A. G.; Gonzalez, J. D. L. *J. Catal.* **1986**, *99*, 171.
(73) Reinoso, F. R.; Ramos, I. R.; Ruiz, A. G.; Gonzalez, J. D. L. *Appl. Catal.* **1986**, *21*, 251.
(74) Hugues, F.; Basset, J. M.; Ben Taarit, Y.; Choplin, A.; Primet, M.; Rojas, D.; Smith, A. K. *J. Am. Chem. Soc.* **1982**, *104*, 7020.
(75) Hugues, F.; Smith, A. K.; Ben Taarit, Y.; Basset, J. M. *J. Chem. Soc., Chem. Commun.* **1980**, 68.
(76) Hugues, F.; Dalmon, J. A.; Bussiere, P.; Smith, A. K.; Basset, J. M. *J. Phys. Chem.* **1982**, *86*, 5136.
(77) Hugues, F.; Besson, B.; Basset, J. M. *J. Chem. Soc., Chem. Commun.* **1980**, 719.
(78) Kuznetsov, V. L.; Danilyuk, A. F.; Kolosova, I. E.; Yermakov, Y. I. *React. Kinet. Catal. Lett.* **1982**, *21*, 249.
(79) Vanhove, D.; Makambo, P.; Blanchard, M. *J. Chem. Soc., Chem. Commun.* **1979**, 605.
(80) Okuhara, T.; Kobayashi, K.; Kimura, T.; Misono, M.; Yoneda, Y. *J. Chem. Soc., Chem. Commun.* **1981**, 1114.
(81) Hallum, J. V.; Drushel, H. V. *J. Phys. Chem.* **1958**, *62*, 110.
(82) Morterra, C.; Low, M. J. D. *Langmuir* **1985**, *1*, 320.
(83) Mattson, J. S.; Mark, H. B.; Weber, W. J. *Anal. Chem.* **1969**, *41*, 355.
(84) Saperstein, D. D. *J. Phys. Chem.* **1986**, *90*, 3883.
(85) Friedel, R. A.; Hofer, L. J. E. *J. Phys. Chem.* **1970**, *74*, 2921.
(86) Kmetko, E. A. *Phys. Rev.* **1951**, *82*, 456.
(87) Zawadzki, J. *Pol. J. Chem.* **1980**, *54*, 979.
(88) Brown, J. K. *J. Chem. Soc.* **1955**, 752.
(89) Friedel, R. A.; Queiser, J. A. *Anal. Chem.* **1956**, *28*, 22.
(90) Ianniello, R. M.; Wieck, H. J.; Yacynych, A. M. *Anal. Chem.* **1983**, *55*, 2067.

although adsorbed CO was recently detected on a 50% Ni/C sample using IR-photothermal beam deflection spectroscopy.[91] This paper shows that DRIFTS can be successfully used to study metal carbonyl clusters and metal particles dispersed on a carbon black. The chemisorption, kinetic, and calorimetric properties of the metal crystallites will first be described; then the DRIFTS results for the clusters and chemisorbed CO will be addressed.

Similar to previous MCC/carbon systems,[19,23,25,26,64] the Os/C catalyst prepared in this study was very well dispersed considering the high metal loading of 9.1 wt % Os. If an adsorption stoichiometry of CO:Os = 1:1 is assumed at 300 K,[32-36] dispersions of 0.6 to 0.7 were obtained for both the fresh and used catalysts after HTR. The CO adsorption values obtained at 195 and 300K were in good agreement, indicating that similar CO coverages occurred at both temperatures. Assuming dissociative H_2 adsorption, the dispersions based on the hydrogen coverages were well within a factor of 2 of the CO-based values. The H_2 desorption procedure developed by Amelse et al.,[92] and previously used for C-supported Fe catalysts,[19,25,26,64] also seems to be applicable to Os/C catalysts. The results clearly show the stability of these C-supported Os particles toward sintering during CO hydrogenation as the adsorption values decreased by only 10%. The highly dispersed and stable nature of Os species supported on oxides such as SiO_2,[13,38,54,60,93] Al_2O_3,[59,60,93-96] and MgO[43,53,97,98] is well-known, but this represents the first report of carbon-supported Os. On oxide supports the stability has been attributed to exceptionally strong interactions between the Os atoms themselves and also between Os atoms and the surface oxygen atoms present on these oxide supports.[59] Since the surface oxygen had been removed from this carbon support, it is presumed that the present stability was due not only to the strong Os–Os bonds, but also to the very high surface area of the amorphous carbon support which provides a large pore volume within very small pores, thereby imposing physical constraints to limit migration and agglomeration. It is also possible that active sites on the carbon surface may have helped obtain the high dispersion and stability.[66]

The kinetic results for CO hydrogenation listed in Table II can be compared to reported values listed in Table VI. The carbon-supported Os catalyst was active after a LTR treatment and remained active after a HTR treatment. Since the IR spectra indicated the presence of CO adsorbed only on reduced Os (no positive-valent Os) after HTR, this activity is attributed to the presence of metallic Os. Methane was essentially the only hydrocarbon product and small amounts of CO_2 were also produced, as expected for supported Os catalysts at low pressures.[43,53,59,99-103] The CH_4 turnover frequency (TOF) at 0.1 MPa over C-supported Os was 2.3×10^{-3} s^{-1} after LTR and 1.5×10^{-3} s^{-1} after HTR, based on the CO uptakes at 300 K. This low TOF shows that Os is much less active than Fe and Ru and is one of the least active group VIII metals for CO hydrogenation.[27] These two TOF values, compared to those for supported Os catalysts after extrapolation of reported values to 1 atm pressure, 548 K, and H_2:CO = 3:1, indicate that carbon-supported Os has a TOF very similar to that of SiO_2-supported Os but one to two orders of magnitude higher than MgO- and Al_2O_3-supported Os. The values obtained by Brenner[100] showed that TOF's on the order of 10^{-5} s^{-1} can be expected for oxidized Os; consequently, a reasonable interpretation of these results is that the MgO- and Al_2O_3-supported Os catalysts were not completely reduced during the measurement of catalytic activities, as would be expected if stable $[Os^{2+}(CO)_2]_n$ or $[Os^{2+}(CO)_3]_n$ (n = 2, 3, ...) surface species were present during reaction conditions. These species have been shown to be the dominant decomposition products of osmium clusters of varying nuclearity on hydroxylated oxide supports.[11,12,15,39,53,59] The higher activities of the SiO_2- and C-supported Os catalysts imply little interaction between the Os and any oxygen groups, thereby facilitating a reduced state of Os prior to and during the CO hydrogenation reaction.

Only one study has dealt with the energetics of the interaction between CO and Os, and it provided an initial heat of adsorption of 33 kcal/mol for CO adsorption on an Os(0001) single crystal.[104] This is in very good agreement with the average Q_{ad} value of 31.3 kcal/mol obtained for this Os/C catalyst. As shown in Table III, this average value was obtained from four measurements on two samples which agreed well and give a standard deviation of 1.1 kcal/mol. As mentioned, the measured chemisorption values remained essentially unchanged and showed the absence of sintering during repeated HTR treatments. The Q_{ad} value obtained on Os is higher than that of 24.2 ± 1.6 kcal/mol on a Ru/C catalyst,[105] which in turn was higher than that of 15.0 ± 1.6 kcal/mol on a Fe/C catalyst.[106] This trend is consistent with that reported for MCC Os–CO, Ru–CO, and Fe–CO bond strengths of 45, 41, and 30 kcal/mol, respectively.[107]

Numerous studies have appeared which deal with the interaction of osmium MCC's of varying nuclearity with oxide supports, and these results are well-summarized.[1,14,100,108] In brief, it has been found that on hydroxylated or partially hydroxylated Al_2O_3, SiO_2, TiO_2, clay, and MgO, a stable $[HOs_3(CO)_{10}(O_s)]$ species (where (O_s) represents a surface oxygen atom) was formed from the interaction of $Os_3(CO)_{12}$ with hydroxyl groups on the surfaces of these materials.[11-15,53,54,59,94-97,109,110] The water content of the support influenced only the rate in which the process occurred and not the chemistry.[11,12,111] Furthermore, this interaction could be reversed by extensive exposure to CO and H_2O, which led to the re-formation of the original cluster.[11,12] The interaction between $Os_3(CO)_{12}$ and highly dehydroxylated MgO gave an $[Os_3(CO)_{11}]^{2-}$ species that interacted ionically with the MgO surface.[11] The decomposition of these supported species led to two proposed final states. On the one hand, numerous authors have reported the formation of $[Os^{2+}(CO)_2]_n$ and $[Os^{2+}(CO)_3]_n$ subcarbonyls on hydroxylated[11-13,15,39,43,53-57,95,96,108-110] and dehydroxylated[11,38] oxide supports. The evidence for these species was obtained from IR spectra[11,12] and EXAFS results, the latter indicating an absence of Os–Os interactions following decomposition.[12] On the other hand, on highly dehydroxylated SiO_2, Al_2O_3, and TiO_2 it was reported that during similar treatments the growth of Os clusters to $[Os_{12}(CO)_{30}C_2]$ occurred, which retained a carbonyl structure but of higher nuclearity.[60,93] The IR spectra, although identical with those reported by Psaro et al. (giving bands at 2120, 2040, and 1960 cm^{-1}), were interpreted by Wells and co-workers not as a pair of overlapping doublets but as three distinct peaks arising due to the interaction of CO with Os^+, Os, and Os^-, all contained within the single, high-nuclearity cluster. The main evidence for this argument was the presence of Os–Os bonds, as observed by UV–visible spectroscopy.[60] In summary, the interaction of $Os_3(CO)_{12}$ with oxide supports has led to the

(91) Low, M. J. D.; Morterra, C.; Severdia, A. G. *Spectrosc. Lett.* **1982**, *15*, 415.
(92) Amelse, J. A.; Schwartz, L. H.; Butt, J. B. *J. Catal.* **1981**, *72*, 95.
(93) Jackson, S. D.; Wells, P. B. *Appl. Catal.* **1986**, *25*, 157.
(94) Deeba, M.; Streusand, B. J.; Schrader, G. L.; Gates, B. C. *J. Catal.* **1981**, *69*, 218.
(95) Knozinger, H.; Zhao, Y. *J. Catal.* **1981**, *71*, 337.
(96) Li, X. J.; Gates, B. C. *J. Catal.* **1983**, *84*, 55.
(97) Choplin, A.; Huang, L.; Theolier, A.; Gallezot, P.; Basset, J. M. *J. Am. Chem. Soc.* **1986**, *108*, 4224.
(98) Lamb, H. H.; Gates, B. C. *J. Am. Chem. Soc.* **1986**, *108*, 81.
(99) Commereuc, D.; Chauvin, Y.; Hughes, F.; Basset, J. M.; Oliver, D. *J. Chem. Soc., Chem. Commun.* **1980**, 154.
(100) Brenner, A. *Metal Clusters*; Wiley: New York, 1986; p 249.
(101) Odebunmi, E. O.; Zhao, Y.; Knozinger, H.; Tesche, B.; Manogue; W. H.; Gates, B. C.; Hulse, J. *J. Catal.* **1986**, *86*, 95.
(102) Hunt, D. J.; Jackson, S. D.; Moyes, R. B.; Wells, P. B.; Whyman, R. *J. Catal.* **1984**, *86*, 333.
(103) Jackson, S. D.; Moyes, R. B.; Wells, P. B.; Whyman, R. *J. Catal.* **1984**, *86*, 342.
(104) Ishi, S. I.; Ohno, Y.; Viswanathan, B. *Surf. Sci.* **1985**, *161*, 349.
(105) Venter, J. J.; Vannice, M. A. *Inorg. Chem.*, in press.
(106) Venter, J. J.; Vannice, M. A. *J. Phys. Chem.*, in press.
(107) Connor, J. A. *Top. Chem.* **1972**, 71.
(108) Gates, B. C. *Metal Clusters*; Wiley: New York, 1986; p 283.
(109) Cook, S. L.; Evans, J.; Greaves, G. N. *J. Chem. Soc., Chem. Commun.* **1983**, 1287.
(110) Schwank, J.; Allard, L. F.; Deeba, M.; Gates, B. C. *J. Catal.* **1983**, *84*, 27.
(111) Giannells, E. P.; Rightor, E. G.; Pinnavaia, T. J. *J. Am. Chem. Soc.*, submitted for publication.

Table VII. Reported Activation Energies and First-Order Rate Constants for Nucleophilic Substitution into $Os_3(CO)_{12}$: $Os_3(CO)_{12-n}L_n + L \rightarrow Os_3(CO)_{11-n}L_{n+1} + CO$

n	L	solvent	ΔH^* (kcal/mol)	rate constant, k_1 ($s^{-1} \times 10^5$)	T (K)	k_1 (min^{-1}) at 350 K	ref
0	CO	decalin	35.0				121
0	L[a]	decalin	33.7				121
0	PPh_3	decalin	32.8				121
0	PBu_3	decalin	33.1				121
0	PPh_3	decalin	31.8				121
0	PBu_3	decalin					121
1	PBu_3	decalin	39.3				121
2	PBu_3	decalin	34.7				121
0	PBu_3	decalin	32.9	7	383	0.00007	121
1	PBu_3	decalin	39.3	3.6	383	0.00002	121
2	PBu_3	decalin	34.7	1.9	383	0.00002	121
0	PPh_3	decane	38.6	1.12	365	0.00007	122
0	$P(OMe)_3$	decane	*b*	1.14	365	0.00007	122
0	PBu_3		*b*	3.36	373	0.00007	122

[a] L = PPh_3, $P(OMe_3)$, $P(Bu)_3$. [b] Assumed $\Delta H^* = 35.6$ kcal/mol.

formation of physisorbed $Os_3(CO)_{12}$, $[HOs_3(CO)_{10}(O_s)]$, $[Os_3(CO)_{11}]^{2-}$, $[Os^{2+}(CO)_{2-3}](O_s)_2$, or $[Os_{12}(CO)_{30}C_2]$, with each species possessing distinct IR frequencies.[13,54,60,96]

The $Os_3(CO)_{12}$ cluster dispersed on carbon gave a spectrum similar to that observed for the cluster in solution. When the cluster was decomposed in flowing He at temperatures between 363 and 433 K, the peak positions remained constant, yet the temperatures used were similar to those at which the transformation of $Os_3(CO)_{12}$ to $[HOs_3(CO)_{10}(O_s)]$ occurs on oxide supports.[11,12] Clearly, the absence of hydroxyl groups on the carbon leads to a mechanism of decomposition different from that observed on oxide supports. Furthermore, the decomposition of $Os_3(CO)_{12}$ on oxide supports like Al_2O_3 was shown to produce oxidized Os,[100,112-115] but the IR spectra obtained after decomposition in He of these clusters on carbon showed only bands associated with CO adsorbed on metallic Os, which is the major end product of decarbonylation in He.

The decarbonylation in H_2 led to the formation of a new species, designated S1, which was formed by the interaction of $Os_3(CO)_{12}$ with H_2, had IR frequencies of 2066 and 2017 cm^{-1}, and could not be attributed to the interaction of $Os_3(CO)_{12}$ with hydroxyl groups. The observed frequencies of various Os carbonyls in solution are given in Table IV, and from this list the species most likely formed during decarbonylation in H_2 was $H_4Os_4(CO)_{12}$, as it is the only species giving just two major bands near 2066 and 2016 cm^{-1}. The frequencies of the anionic species are too low, and, more importantly, the frequencies of the species formed on oxide supports do not match the frequencies of S1.

The formation of $H_4Os_4(CO)_{12}$ from $Os_3(CO)_{12}$ in H_2 requires an increase in cluster nuclearity and the incorporation of H_2 into the cluster; both of these reactions have been previously observed. An increase in cluster nuclearity was observed when $Rh_6(CO)_{16}$, $Rh_4(CO)_{12}$, and $Rh_2(CO)_4Cl_2$ were impregnated on an Al_2O_3 support. Extraction of adsorbed species in $CHCl_3$ showed the presence of only $Rh_6(CO)_{16}$ in all three cases, which suggested surface migration and reconstruction following the impregnation.[100,116] More conclusively, the increase in nuclearity of Os clusters in solution in the presence of H_2 is well-documented;[46,51,117,118] therefore, the assumption of an increase in cluster nuclearity is quite reasonable. The incorporation of H_2 into supported clusters has also been observed; for example, $H_2RuOs_3(CO)_{13}$ supported on Al_2O_3 formed the expected $[HRuOs_3(CO)_{13}]^-$ anion, which interacts with surface cations. Flowing CO and H_2 over this catalyst transformed this cluster to $[H_3RuOs_3(CO)_{12}]^-$ through the reversible incorporation of H_2.[119] Incorporation of H_2 into Os MCC's in solution is also known,[46,51,117,118] and the most important of these studies is that of Knox et al.,[46] who observed the reaction proposed here, i.e., the transformation of $Os_3(CO)_{12}$ to $H_2Os_3(CO)_{10}$ and then to $H_4Os_4(CO)_{12}$ in 1 atm of flowing H_2 at 393 K in an octane solvent. Perhaps the most convincing evidence for this reaction comes from the work of Lamb and Gates,[43,98] who supported $H_2Os(CO)_4$, $H_4Os_4(CO)_{12}$, and $Os_6(CO)_{18}$ on MgO and subjected these clusters to CO hydrogenation at 10 atm. The resulting catalysts contained only two species, namely $[H_3Os_4(CO)_{12}]^-$ and $[Os_{10}C(CO)_{24}]^{2-}$, showing that cluster reconstruction and H_2 incorporation had occurred. This previous work, together with the agreement between the observed and reported IR frequencies, leads to the conclusion that the $H_4Os_4(CO)_{12}$ species is the most likely one formed during decomposition of $Os_3(CO)_{12}$.

The decarbonylation in He and H_2 proceeded via different paths, since no stable carbonyl species other than the original $Os_3(CO)_{12}$ was observed in flowing He. Several studies have appeared dealing with nucleophilic substitution reactions of $Os_3(CO)_{12}$.[120-122] The interaction of $Os_3(CO)_{12}$ with a nucleophilic ligand, L, usually leads either to substitution of CO with L yielding $Os_3(CO)_{12-n}L_n$ (n = 1, 2, 3)[120] or to cluster fragmentation yielding reduced, mononuclear Os species.[121] The relative importance of these two mechanisms depends strongly on the nature and concentration of L, as low concentrations of PPh_3 [$P(C_6H_5)_3$] lead primarily to substitution,[122] whereas high concentrations of PBu_3 [$P(C_4H_9)_3$] lead exclusively to mononuclear species.[121] The overall mechanism of this process can be summarized as shown in Scheme A of Figure 9. Either substitution or fragmentation reactions, however, depend on an initial rate-determining rupture of a single Os–CO bond.[120] This initial bond rupture, in turn, can proceed through two mechanisms, i.e., an associative mechanism where the rupture of the Os–CO bond occurs during or after the incorporation of L, or a dissociative mechanism where the rupture of the Os–CO bond occurs first. These two mechanisms then lead to an observed rate constant of the form $k_0 = k_1 + k_2[L]$, where k_1 is the constant for the first-order dissociative mechanism and k_2 is the constant for the second-order associative mechanism. Again, the relative importance of these two terms depends on the nature and concentration of L.[120] Reported rates of substitution into $Os_3(CO)_{12}$ and their associated kinetic parameters are listed in Table VII. They show that a first-order rate constant of 0.000 07 min^{-1} at 350 K is consistently found for substitution into $Os_3(CO)_{12}$, and that this rate constant is relatively insensitive to the solvent and does not decrease markedly as the extent of substitution increases, i.e., n = 1 and 2. Furthermore, this reported value for the original

(112) Brenner, A.; Hucul, A. *J. Am. Chem. Soc.* **1980**, *102*, 2484.
(113) Hucul, D. A.; Brenner, A. *J. Am. Chem. Soc.* **1981**, *103*, 217.
(114) Brenner, A.; Hucul, A. *Inorg. Chem.* **1979**, *18*, 2836.
(115) Hucul, D. A.; Brenner, A. *J. Phys. Chem.* **1981**, *85*, 496.
(116) Smith, G. C.; Chojnacki, T. P.; Iwatate, K.; Watters, K. L. *Inorg. Chem.* **1975**, *14*, 1419.
(117) Kaesz, H. D.; Saillant, R. B. *Chem. Rev.* **1972**, *72*, 231.
(118) Johnson, B. F. G.; Lewis, J.; Raithby, P. R.; Sheldrick, G. M.; Suss, G. *J. Organomet. Chem.* **1978**, *162*, 179.
(119) Budge, J. R.; Scott, J. P.; Gates, B. C. *J. Chem. Soc., Chem. Commun.* **1983**, 342.
(120) Poe, A. J. *Metal Clusters*; Wiley: New York, 1986; p 53.
(121) Poe, A. J.; Sekhar, V. C. *Inorg. Chem.* **1985**, *24*, 4376.
(122) Sohjaie, A.; Atwood, J. D. *Organometallics* **1985**, *4*, 187.

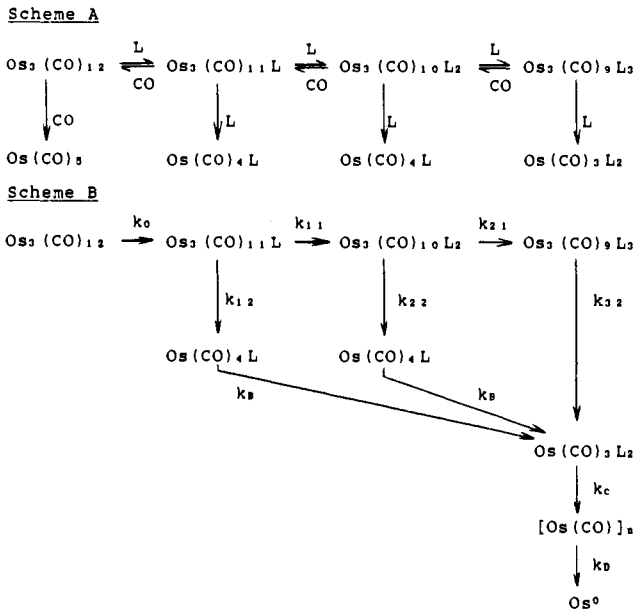

Figure 9. Proposed mechanism for the decomposition of carbon-supported $Os_3(CO)_{12}$ in He.

cluster is within a factor of 2 or 3 of the rate constants in Table V for decarbonylation of carbon-supported $Os_3(CO)_{12}$ clusters. This provides strong evidence that the decarbonylation of $Os_3(CO)_{12}$/C proceeds via a similar mechanism.

The rate constants for substitution into $Os_3(CO)_{11}L$ and $Os_3(CO)_{10}L_2$ are not much lower than the values for $Os_3(CO)_{12}$,[122] and it is well-stablished that the relative reactivity of group VIII metals toward nucleophilic substitution is $Fe_3(CO)_{12} > Ru_3(CO)_{12} > Os_3(CO)_{12}$, but for the pentacarbonyls it is $Os(CO)_5 > Ru(CO)_5 > Fe(CO)_5$. Therefore, the likelihood of detecting stable, mononuclear complexes is greatest for Fe and least for Os. Consistent with this trend, no mononuclear complex was observed during the decarbonylation of $Os_3(CO)_{12}$. To address the question of whether any substitution intermediates could be present in sufficiently high concentrations to be detected by IR, the decarbonylation of $Os_3(CO)_{12}$ was modeled using a set of coupled, first-order differential equations derived from Scheme B in Figure 9. The calculated IR intensities of all these species as a function of time, assuming a constant extinction coefficient for the carbonly band, is shown in Figure 10, in which all rate constants were equal to 0.0002 min^{-1} except k_0, which was 0.0007 min^{-1}. The resulting plots indicate that no species with nuclearity equal to or less than 3 should give an intensity greater than 15% of the original intensity of $Os_3(CO)_{12}$, which is behavior consistent with that observed in He. The marked increase in intensity of a species, as observed in H_2, cannot be explained by this mechanism and is consistent with the formation of a new species, $H_4Os_4(CO)_{12}$.

The measured activation energies of decarbonylation of 27–29 kcal/mol in He and 30–33 kcal/mol in H_2 are slightly lower than the values reported for nucleophilic substitution (Table VII). These lower activation energies can be explained if rapid Os–Os bond formation occurs during decarbonylation, and two limiting thermodynamic pathways can be constructed to calculate the minimum activation energy for this endothermic process, as shown in Figure 11. Case 1 represents $n[Os_3(CO)_{12}]$ molecules decomposing to form gas-phase CO and a hexagonal close-packed Os crystal phase. The Os–CO and Os–Os bond energies were taken as 45 and 31 kcal/mol, respectively,[107] whereas the condensation energy was taken as the Os cohesive energy density of 188 kcal/mol.[123] Using these values, a minimum activation energy of 6 kcal/mol is obtained, which is significantly lower than the measured values. Case 2 represents the formation of highly dispersed metallic Os particles in which the Os–Os bond strength

(123) Kittel, C. *Introduction to Solid State Physics*; Wiley: New York, 1976.

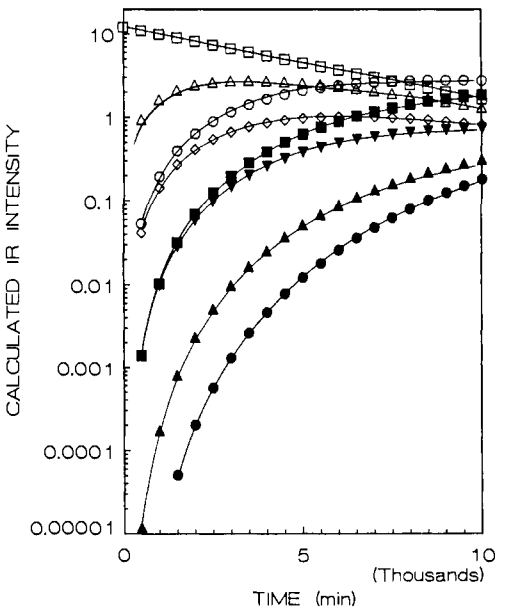

Figure 10. Evolution of substitution products for Scheme B. The IR intensities were calculated assuming equal extinction coefficients for all CO ligands present, with a basis of 1 mol of $Os_3(CO)_{12}$: □, $Os_3(CO)_{12}$; △, $Os_3(CO)_{11}L$; ◇, $Os_3(CO)_{10}L_2$; ▼, $Os_3(CO)_9L_3$; ○, $Os(CO)_4L$; ■, $Os(CO)_3L_2$; ▲, $[Os(CO)]_n$; ●, Os.

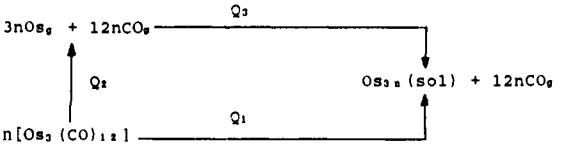

Heat of Transformation:

$Q_1(tot) = Q_2 + Q_3$
$= (-3nE_{Os-Os} - 12nE_{Os-CO}) + (E_{formation\ of\ solid}$
$Q_1(per\ CO) = -)3nE_{Os-Os} + 12nE_{Os-CO})/12n + (E_{cond})/12n$
For E_{Os-Os}=31 kcal/mole and E_{Os-CO}=45 kcal/mole (Ref. 107)
$Q_1(per\ CO) = -52.8 +)E_{cond})/12n$

CASE 1: Formation of Bulk Os Metal.

$E_{cond} = +(3nE_{cohesive\ energy\ density})/12n$
But $E_{cohesive\ energy\ density}$=188 kcal/mole (Ref. 123)
$E_{cond} = +3(188)/12 = +47$ kcal/mole.
$Q_1 = -52.8 + 47 = -6$ kcal/mole.

CASE 2: Formation of Os Clusters.

$E_{cond} = +(0.5*z*3n*E_{Os-Os})/12n$
$= +zE_{Os-Os}/8$
$= +3.875z$
$Q_1(per\ CO) = -52.8 + 3.875z$
for Q_1 (per CO)=-27.3 to -32.5 kcal/mole, z=7-8 nearest neighbors.

Figure 11. Thermodynamic path to estimate the minimum activation energy for the endothermic decarbonylation of $Os_3(CO)_{12}$. E_{Os-Os} is the Os–Os bond strength in $Os_3(CO)_{12}$; E_{cond} is the energy released during the formation of an Os particle; E_{Os-CO} is the Os–CO bond strength in $Os_3(CO)_{12}$; z is the number of nearest neighbors in the Os particles.

remains similar to that observed in $Os_3(CO)_{12}$. The number of nearest neighbors, z, required to give the measured activation energies of 27.3–32.5 kcal/mol can then be calculated as shown in Figure 11. This estimate yields values for z of 5 to 7, which are very reasonably for surface Os atoms in a very small crystallite (1 nm, for example).

Metallic Os particles were obtained after decarbonylation of $Os_3(CO)_{12}$ in either He or H_2, as evidenced by a single CO absorption band at 2035–2037 cm^{-1}, in good agreement with previous spectra of CO adsorbed on reduced Os.[12,59,60] Os oxide gives rise to $[Os^{2+}(CO)_2]_n$ and $[Os^{2+}(CO)_3]_n$ species with frequencies at 2045 and 1960 cm^{-1}, and 2120 and 2037 cm^{-1}, respectively.[11,12]

The absence of such bands, as expected for a surface free of surface hydroxyl groups,[64] indicates no detectable amount of Os oxide was present.

The spectra under reaction conditions, shown in Figure 8, indicate an increase in intensity in the region associated with CH_x bands with increasing temperature and time on-stream. The adsorbed CO species, giving a broad band between 2030 and 1950 cm^{-1} at these temperatures, decreased in intensity with increasing temperature as anticipated for equilibrated surface coverage. Previous studies on Fe/SiO_2 and Ru/SiO_2 have investigated the 2700–3100-cm^{-1} range, and it has been routinely concluded that most of the species providing the observed CH_x bands are present on the support and not on the metal surface.[61,124,125] Furthermore, since only frequencies at 2930 and 2850 cm^{-1} were observed, CH_2 groups predominated and were attributed to higher molecular weight saturated hydrocarbon chains, in agreement with the known capability of Ru and Fe catalysts to form longer chain hydrocarbons.[126,127] In the present study on carbon-supported Os, approximately equal quantities of CH_2 and CH_3 species were present, as seen by a comparison of the 2927- and 2862-cm^{-1} doublet for CH_2 stretching frequencies, and the 2962- and 2872-cm^{-1} doublet for CH_3 stretching frequencies. This indicates a preponderance of short-chain hydrocarbons which exist possibly on the Os surface, but more likely on the carbon surface within the small pore structure. However, at a given temperature the CH_x intensities and the CO intensity seem to be inversely related, and since the CO is present only on the Os surface, this provides indirect evidence that at least a portion of the detected CH_2 and CH_3 species may have been present on the Os surface.

Summary

A carbon-supported metal catalyst has been characterized by IR spectroscopy for the first time, as DRIFTS, along with a modified controlled environment cell, was successfully applied to study carbon-supported Os clusters. The decarbonylation of $Os_3(CO)_{12}$ on oxygen-free carbon surfaces was followed quantitatively to obtain first-order rate constants and activation energies of decarbonylation of 27–29 kcal/mol in He and 30–33 kcal/mol in H_2. To the best of our knowledge, this is the first time that the kinetics of thermal decomposition of $Os_3(CO)_{12}$ has been determined. The activation energies are slightly lower than those reported for nucleophilic substitution reactions of $Os_3(CO)_{12}$ in solution; however, the assumption of rapid formation of Os–Os bonds to produce small metallic Os particles allowed an estimation of activation energies based on known Os–Os and Os–CO bond strengths that were consistent with the values measured. Decarbonylation in He proceeded to Os metal without the formation of stable intermediates, whereas decomposition in H_2 first produced $H_4Os_4(CO)_{12}$, which then decomposed to Os metal.

CO adsorption on the carbon-supported Os crystallites after decomposition in either H_2 or He yielded spectra in excellent agreement with literature values of 2035–2037 cm^{-1} for CO adsorbed on metallic Os surfaces. IR spectra under reaction conditions showed the presence of adsorbed CO as well as similar concentrations of CH_2 and CH_3 groups which indicated the presence of only short-chain hydrocarbons on the catalyst surface. The integral heat of adsorption of CO at 300 K on these metallic Os crystallites was determined calorimetrically to be 31.3 ± 1.1 kcal/mol, in good agreement with the value of 33 kcal/mol reported for CO adsorption on an Os(0001) single crystal. The chemisorption measurements showed that the Os particles were well-dispersed and resistant to sintering under reaction conditions. The turnover frequency for methanation, the only hydrocarbon product detected, was similar to that on well-reduced Os/SiO_2 catalysts, but much higher than TOF values reported for Os on Al_2O_3 and MgO where Os remains in a stabilized, positive-valent state. Regardless, even the best Os catalysts have low turnover frequencies for CO hydrogenation compared to the most active group VIII metals, such as Ru and Fe, which lie just above Os in the periodic table.

Acknowledgment. This study was supported by the donors of the Petroleum Research Fund, administered by the American Chemical Society.

Registry No. $Os_3(CO)_{12}$, 15696-40-9; $H_4Os_4(CO)_{12}$, 12375-04-1; H_2, 1333-74-0; CO, 630-08-0.

(124) Ekerdt, J. G.; Bell, A. T. *J. Catal.* **1979**, *58*, 170.
(125) Ekerdt, J. G.; Bell, A. T. *J. Catal.* **1979**, *62*, 19.
(126) Vannice, M. A. *Catal. Rev. Sci. Technol.* **1976**, *14*, 153.
(127) Boudart, M.; McDonald, M. A. *J. Phys. Chem.* **1984**, *88*, 2185.

Gas-Phase Study of Fe^+–Benzyne with Alkanes

Yongqing Huang and Ben S. Freiser*

Contribution from the Department of Chemistry, Purdue University, West Lafayette, Indiana 47907. *Received August 1, 1988*

Abstract: The unimolecular chemistry of Fe^+–benzyne and its reactivity with small alkanes in the gas phase are studied by Fourier transform mass spectrometry (FTMS). Collision-induced dissociation of Fe^+–benzyne yields benzyne loss exclusively. In contrast, photodissociation of Fe^+–benzyne yields not only cleavage of benzyne from Fe^+, but competitive loss of C_2H_2 and C_4H_2 as well. The Fe^+–benzyne is formed from chlorobenzene by loss of HCl. This dehydrochlorination of chlorobenzene also occurs in secondary reactions up to six times forming products of the type Fe^+–polyphenylene. Fe^+–benzyne reacts with alkanes larger than methane to form a wide variety of product ions by mechanisms including hydrogenation and methanation of the benzyne ligand. All of the product ions can be explained by mechanisms based on Fe^+ insertion into either C–C or C–H bonds as the reaction-initiating step, followed by either alkyl or H migration from Fe^+ onto the benzyne ligand or, alternatively, by the migratory insertion of benzyne into a metal–carbon or metal–hydrogen bond. Photodissociation and ion–molecule reaction studies yield a value for the metal–ligand bond energy of $D°(Fe^+$–benzyne) = 76 ± 10 kcal/mol.

Recent studies on bare gas-phase transition metal cations M^+ have provided abundant information on their reactivities and mechanisms with a wide variety of organic compounds.[1] A logical extension of this work has been to compare the results obtained from studies on ML_n^+ (L = ligand, $n \geq 1$) with that of the bare metal species in order to gain an understanding of the intrinsic effect of the ligand on the reactivity of the metal center.[2,3] Studies thus far have included a wide variety of small ligands (e.g., H,

(1) For a recent review, see: Allison, J. In *Progress in Inorganic Chemistry*; Lippard, S. J., Ed.; Wiley-Interscience: New York, 1986; Vol. 34, p 628 and references therein.

(2) Freas, R. B.; Ridge, D. P. *J. Am. Chem. Soc.* **1980**, *102*, 7129.
(3) Some examples are: Jacobson, D. B.; Freiser, B. S. *J. Am. Chem. Soc.* **1984**, *106*, 3891; **1985**, *107*, 67. Cassady, C. J.; Freiser, B. S. *J. Am. Chem. Soc.* **1984**, *106*, 6176. Jackson, T. C.; Jacobson, D. B.; Freiser, B. S. *J. Am. Chem. Soc.* **1984**, *106*, 1252.

0002-7863/89/1511-2387$01.50/0